Modeling of dendritic growth using a quantitative nondiagonal phase field model

Kai Wang,[1] Guillaume Boussinot,[2] Claas Hüter,[1] Efim A. Brener,[3] and Robert Spatschek[1,4]
[1]*Institute for Energy and Climate Research, IEK-2, Forschungszentrum Jülich, D-52425 Jülich, Germany*
[2]*Access e.V., Intzestrasse 5, 52072 Aachen, Germany*
[3]*Peter Grünberg Institut, Forschungszentrum Jülich, D-52425 Jülich, Germany*
[4]*JARA-ENERGY, 52425 Jülich, Germany*

(Received 2 January 2020; accepted 28 February 2020; published 19 March 2020)

The phase field method has emerged as the tool of choice to simulate complex pattern formation processes in various domains of materials sciences. For the phase field model to faithfully reproduce the dynamics of a prescribed free-boundary problem with transport equations in the bulk and boundary conditions at the interfaces, the so-called thin-interface limit should be performed. For a phase transformation driven by diffusion, the kinetic cross-coupling between the phase field and the diffusion field has recently been introduced, allowing a control on interface boundary conditions in the general case where the diffusivity in the growing phase D_S neither vanishes (one-sided model) nor equals the one of the disappearing phase D_L (symmetric model). Here, we investigate the capabilities of this nondiagonal phase field model in the case of two-dimensional dendritic growth. We benchmark our model with Green's function calculations (sharp-interface model) for the symmetric and one-sided cases, and our results for arbitrary D_S/D_L allow us to propose a generalization of the theory by Barbieri and Langer [Phys. Rev. A **39**, 5314 (1989)] for finite anisotropy of interface energy. We also perform simulations that evidence the necessity of introducing the kinetic cross-coupling and of eliminating surface diffusion. Our work opens up the way for quantitative phase field simulations of phase transformations with diffusion in the growing phases playing an important role in the pattern and velocity selections.

DOI: 10.1103/PhysRevMaterials.4.033802

I. INTRODUCTION

The phase field (PF) method has emerged in the last 30 years as one of the most powerful tools to tackle free boundary problems in various fields [1–5]. While in free boundary problems, different bulk domains where transport equations hold are separated by interfaces with boundary conditions, the PF models describe continuous fields obeying the same evolution equations everywhere in space, with the spatial variations of the so-called PF (nothing but an order parameter) representing the interfaces. The latter thus possesses a certain width which is a numerical parameter that has no physical meaning. To simulate extended systems, the interface width needs to be chosen orders of magnitude larger than the physical width of the interface (of the order of the atomic distance). Since, of course, the field dynamics are influenced by the interface width, special care thus has to be taken for the PF model to reproduce a desired free boundary problem.

In Ref. [6], an asymptotic analysis linking the classical PF model (model C in the Hohenberg-Halperin nomenclature [7]) and the free boundary problem was introduced and named the *thin-interface limit*. On the one hand, the thin-interface analysis provides the influence of the parameters of the PF model on the conservation equation at the moving interface (Stefan condition). On the other hand, it provides the link with the kinetic coefficients describing the deviation from local equilibrium at the interface. In particular, the thin-interface analysis allows one to choose the PF model parameters so as to reproduce local equilibrium boundary conditions that are relevant to usual solidification experiments as well as industrial processes such as casting.

While designed for a transformation driven by heat diffusion in a pure material with equal diffusivity in both phases (symmetric model), the thin-interface limit was later on performed in the case of alloys with a vanishing diffusivity in the growing solid phase (one-sided model) [8]. Equilibrium boundary conditions were then shown to require the addition of a so-called *anti-trapping current* in the equation for the alloy concentration. However, in the general case where the diffusivity of the growing phase D_S neither equals the one of the disappearing phase D_L nor vanishes, the thin-interface analysis of the classical PF model shows that equilibrium boundary conditions may not be achieved without altering the thermodynamics of the interface with some unphysical adsorption [9]. Only recently, this problem has been solved [10] by the introduction of the kinetic cross-coupling between the PF and the diffusion field [11]. In the constitutive force-flux relations of the PF model, cross terms are then present, and are parametrized by the same new parameter, according to Onsager's symmetry. This new parameter provides the additional degree of freedom to achieve equilibrium boundary conditions at the interface. We note that these cross terms have been shown to also be responsible for the Ehrlich-Schwoebel effect in the nondiagonal PF model for molecular-beam-epitaxy [12].

Assuming a finite diffusivity in the growing phase differing from the one in the disappearing phase is also highly relevant to pure materials for which the thermal diffusivity is generically different in the different phases. In alloys, where the chemical diffusion coefficient is usually much smaller in the solid than in the liquid for a substitutional solute, but it may be

of the same order in solid and liquid for an interstitial solute such as carbon in steels. Moreover, for alloys in general, solid-state transformations such as the eutectoid reaction are best described using a finite contrast of the diffusion coefficient [13,14].

In this paper, we apply the nondiagonal PF model to the problem of two-dimensional dendritic growth. The dendritic problem represents an archetype of a pattern formation process described by nonlinear dynamics, and it represents a kind of standard benchmark problem for PF models. The development of the dendritic theory comprised two stages. First, Ivantsov described a parabolic dendrite tip in absence of interface energy [15]. Within this frame, the relation between the undercooling and the Péclet number (product of the tip radius and the steady-state velocity) is found, ensuring the conservation of energy around the parabolic tip. Second, it was shown around 30 years later that a solution exists, i.e., the tip radius and the velocity selected separately, only in the presence of interface energy anisotropy (see Ref. [16] and references therein). Some time was additionally required to solve the problem in three dimensions [17,18]. These studies were performed within a symmetric model where the diffusivity is the same for both phases. In Ref. [19], the selection theory was extended to arbitrary ratios of diffusivity $\mu = D_S/D_L$. The μ dependence of the velocity was found analytically in the limit of vanishing anisotropy, while for larger anisotropies, a numerical resolution of the boundary integral equation [Green's function (GF) method] is needed. However, until now, these numerics were performed only for the symmetric ($\mu = 1$) and the one-sided ($\mu = 0$) models, for which the integral equation simplifies drastically. Here, using Green's function calculations for $\mu = 0$ and $\mu = 1$, we come up with a μ dependence of the velocity to which we confront our PF simulations for different μ. We find that the nondiagonal PF model reproduces quantitatively the Green's function results for $\mu = 0$ and $\mu = 1$, and matches well the suggested μ dependence, when the undercooling is small enough. Also, we evidence the importance of the kinetic cross-coupling using simulations within the classical PF model. Finally, we additionally confirm the importance of the procedure for eliminating surface diffusion, as described in detail in Ref. [20].

II. NONDIAGONAL PHASE FIELD MODEL

In the present paper, the main difference to the PF model described in Refs. [10,20] concerns the angular dependence of the interface energy, responsible for the existence of the dendritic solution. In two dimensions, the normal direction $\mathbf{n}$ to the interface is a function of the space coordinates x and y, and only one parameter describes the anisotropy of interface energy. In terms of the PF model, this anisotropy enters the interface width through the partial derivatives of the PF $\phi(x, y)$ [6]:

$$W(\mathbf{n}) = W_0(1-3\epsilon)\left[1 + \frac{4\epsilon}{1-3\epsilon}\frac{(\partial_x\phi)^4 + (\partial_y\phi)^4}{|\nabla\phi|^4}\right].$$

ϵ represents the strength of the fourfold anisotropy and W_0 indicates the average value of the interface width.

Then, Eq. (9) in Ref. [10] is rewritten as

$$\begin{aligned}\mathcal{D}\mathrm{et}(\mathbf{n})\tau(\mathbf{n})\dot{\phi} = H\Big\{&\phi(1-\phi^2) + \nabla\cdot[W^2(\mathbf{n})\nabla\phi] \\ &+ \partial_x\left(|\nabla\phi|^2 W(\mathbf{n})\frac{\partial W(\mathbf{n})}{\partial(\partial_x\phi)}\right) \\ &+ \partial_y\left(|\nabla\phi|^2 W(\mathbf{n})\frac{\partial W(\mathbf{n})}{\partial(\partial_y\phi)}\right)\Big\} \\ &- \frac{p'(\phi)}{2}u + M(\mathbf{n})W(\mathbf{n})D(\phi)\nabla\phi\cdot\nabla u \quad (1)\end{aligned}$$

and the second equation for the diffusion field u (Eq. (10) in Ref. [10]) reads

$$\dot{u} = \nabla\cdot\{D(\phi)[\nabla u + M(\mathbf{n})W(\mathbf{n})\dot{\phi}\nabla\phi]\} + \frac{p'(\phi)}{2}\dot{\phi}. \quad (2)$$

For a pure material, $u = (T - T_M)c_P/L$ measures the deviation of the temperature T from the melting temperature T_M, with c_P and L being the specific heat and latent heat, respectively. Similarly, for the solidification of a binary alloy at a given temperature, $u = (C - C_L)/(C_S - C_L)$ measures the deviation of the concentration C from the liquidus concentration C_L, with C_S being the solidus concentration. On the right-hand side of Eq. (1), the term parametrized by the dimensionless H comes from the ϕ dependence of the thermodynamics of the system. The first term is inherited from the double well potential, with minima at $\phi = \pm 1$ and a maximum at $\phi = 0$, while the second, third, and fourth terms represent the $\mathbf{n}$-dependent penalization of ϕ variations. Here, in comparison to Refs. [10,20], the relaxation time τ, the cross-coupling parameter M and, as a consequence, the determinant (that has to be positive) $\mathcal{D}\mathrm{et} = 1 - (MW\nabla\phi)^2 D(\phi)/\tau$, present an explicit dependence on the orientation of the interface. This dependence is related to the choice of interface conditions that we aim to reproduce with the PF model, whose dynamics is highly influenced by W as mentioned in the Introduction. Our model is called nondiagonal owing to the existence of the terms parametrized by M. In opposition, for a diagonal model, one has $M = 0$. These additional contributions appear as a consequence of nondiagonal terms in the force-flux Onsager relations describing the dynamics of the system. They yield a kinetic cross-coupling between the nonconserved field ϕ and the conserved field u. The Onsager relations give the proportionality between two fluxes (flux of heat and flux of matter across the interface for the thermal model, diffusion flux, and interface velocity for the alloy model) and two driving forces (temperature gradient and jump of free energy at the interface for the thermal model, gradient of diffusion chemical potential, and jump of grand potential for the alloy model) [12]. Only one of the two fluxes exists in the bulk, but both exist at the interface, leading to a 2×2 matrix of interface kinetic coefficients. As will be shown explicitly later, a finite value M is necessary to reproduce equilibrium conditions at the interface when the diffusion coefficients are finite in both phases and different. One should note that, when the diffusion flux vanishes in the bulk solid (one-sided case with $D_S/D_L = 0$), the Onsager symmetry may not be invoked because the two fluxes at the interface are not linearly independent. This gives

the possibility to introduce the term parametrized by M only in Eq. (2), presented as an antitrapping term by Karma [8].

At equilibrium ($u = 0$), the one-dimensional PF profile reads $\phi_{\rm eq}(x) = -\phi_{\rm eq}(-x) = \tanh(x/\sqrt{2}W)$. In the following, we assign the equilibrium value $\phi = 1$ to the growing phase (solid phase) and $\phi = -1$ to the disappearing phase (liquid phase). Within this frame, the orientation-dependent capillary length, reflecting the orientation dependence of interface energy, is $d(\mathbf{n}) = \alpha H W(\mathbf{n})$ where $\alpha = W\int_{-\infty}^{\infty} dx[\phi'_{\rm eq}(x)]^2 = 2\sqrt{2}/3$ is independent of $\mathbf{n}$. For a pure material, the function $p(\phi)$ interpolates between the values at the melting temperature of the solid and liquid entropies [10]. For a binary alloy, $p(\phi)$ interpolates between the equilibrium values of the concentration field [12]. We choose an odd function $p(\phi) = -p(-\phi) = 15(\phi - 2\phi^3/3 + \phi^5/5)/8$ for which $p(\phi = \pm 1) = \pm 1$. The oddness of $p(\phi)$ ensures the absence of undesired adsorption effects at the interface.

The diffusivity is phase dependent (D_S in solid and D_L in liquid) through its ϕ-dependence. Some of the authors have shown [10] that to reproduce equilibrium boundary conditions at the interface, one may use a diffusivity that reads

$$\frac{1}{D(\phi)} = \left(\frac{1}{2D_S} + \frac{1}{2D_L}\right) + g(\phi)\left(\frac{1}{2D_S} - \frac{1}{2D_L}\right), \tag{3}$$

where the odd function $g(\phi) = -g(-\phi)$ also obeys $g(\pm 1) = \pm 1$. In addition, in order not to alter the heat/mass conservation equation at the moving interface with a surface diffusion flux, $g(\phi)$ should incorporate some contribution parametrized by a coefficient a that depends on $\mu = D_S/D_L$, and chosen such that $\int_{-\infty}^{\infty} dx\{D[\phi_{\rm eq}(x)] - D_S/2 - D_L/2\} = 0$ [9]. As in Ref. [20], we choose a function g of the form $g(\phi) = \phi[1 + a(1 - \phi^2)]$. Then for each μ, one should find the coefficient a^* such that the above-mentioned integral vanishes.

To achieve equilibrium boundary conditions, the relaxation time and the cross-coupling coefficient read

$$\tau(\mathbf{n}) = \frac{\beta W^2(\mathbf{n})}{4\alpha}\left(\frac{1}{2D_S} + \frac{1}{2D_L}\right), \tag{4}$$

$$M(\mathbf{n}) = \frac{\chi W(\mathbf{n})}{2\alpha}\left(\frac{1}{2D_S} - \frac{1}{2D_L}\right), \tag{5}$$

where $\beta = \int_{-\infty}^{\infty}(dx/W)\{1 - p^2[\phi_{\rm eq}(x)]\} \simeq 1.40748$ and $\chi = \int_{-\infty}^{\infty}(dx/W)\{1 - p[\phi_{\rm eq}(x)]g[\phi_{\rm eq}(x)]\}$. Here, we note the necessity of introducing a nondiagonal model to simulate $D_S \neq D_L$ with D_S and D_L being finite, while a diagonal model with $M = 0$ is sufficient when $D_S = D_L$. Since $g(\phi)$ varies with μ through the variation of a^*, the value of χ also depends on μ. In Fig. 1, we present a^* and χ in the range of μ that the present model allows us to investigate. Indeed, due to the condition of positiveness of the determinant $\mathcal{D}$et, we have an upper bound for the absolute value of M, that in turns sets the lower bound to the ratio μ (here close to 0.06) for which we are able to achieve equilibrium boundary condition and elimination of surface diffusion [10,20]. It is also important to notice that a^* and χ obey $a^*(\mu) = a^*(1/\mu)$ and $\chi(\mu) = \chi(1/\mu)$.

As mentioned in the Introduction, in this paper we are also interested in the one-sided case where $\mu = 0$. Then, one has to use another definition of the diffusivity than Eq. (3). Instead,

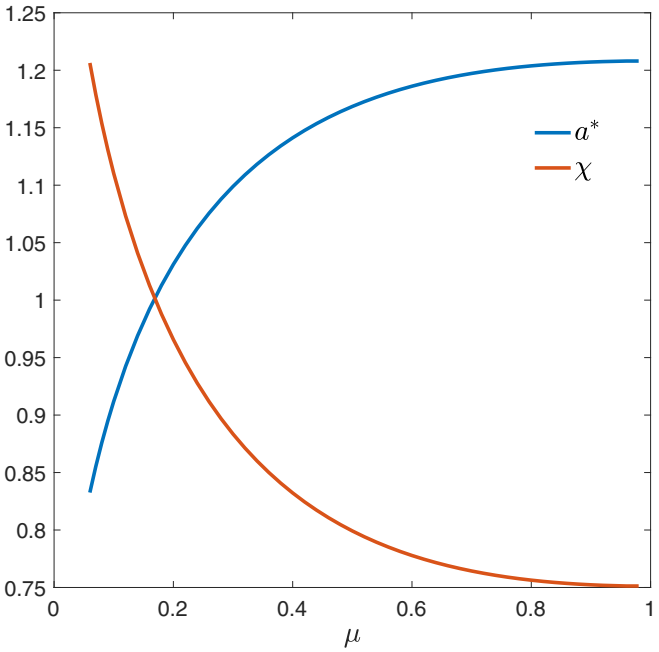

FIG. 1. Selected value a^* of the parameter a in the function $g(\phi)$ such that surface diffusion is eliminated, and corresponding value of χ.

we write

$$D(\phi) = D_{os}(\phi) = D_L(1 - \phi)/2. \tag{6}$$

In Ref. [12], the equilibrium boundary conditions have been reproduced when (please pay attention to the fact that in Ref. [12] we use a double well potential yielding equilibrium values for the PF $\phi = 1$ and $\phi = 0$)

$$M(\mathbf{n}) = M_{os}(\mathbf{n}) = \frac{\zeta W(\mathbf{n})}{2\alpha D_L}, \tag{7}$$

$$\tau(\mathbf{n}) = \tau_{os}(\mathbf{n}) = \frac{\lambda W^2(\mathbf{n})}{4\alpha D_L}, \tag{8}$$

where $\zeta = \int_{-\infty}^{\infty}(dx/W)\{1 + \phi_{\rm eq}(x) - 2p[\phi_{\rm eq}(x)]\}/[1 - \phi_{\rm eq}(x)] \simeq 2.12132$ and $\lambda = 2\int_{-\infty}^{\infty}(dx/W)\{1 - p^2[\phi_{\rm eq}(x)]\}/[1 - \phi_{\rm eq}(x)] \simeq 3.42778$. Here, we note that surface diffusion is suppressed with the choice in Eq. (6) since $\int_{-\infty}^{\infty} dx\{D_{os}[\phi_{\rm eq}(x)] - D_L/2\} = 0$.

III. BOUNDARY INTEGRAL EQUATIONS

As mentioned in the Introduction, we also have performed boundary integral calculations in this paper. The boundary integral technique consists of writing an integro-differential equation for the steady state of interface shape $y_{\rm int}(x)$. While for an arbitrary shape of the interface, the diffusion field is obtained through an integral over the interface of a kernel involving the GF of the diffusion equation, the solution $y_{\rm int}(x)$ is determined by imposing the value $u_{\rm int}$ of the diffusion field u at the interface, here with the Gibbs-Thomson local equilibrium condition,

$$u_{\rm int} = \Delta - d_0(1 - 15\epsilon\cos 4\theta)\kappa. \tag{9}$$

Δ represents the value of the dimensionless diffusion field at infinity ahead of the growing dendrite, d_0 represents the average value of the capillary length (related to the parameters of the PF model through $d_0 = \alpha H W_0$), ϵ is the anisotropy parameter in Eq. (1), and $\kappa = -y''_{\rm int}/(1 + y'^2_{\rm int})^{3/2}$ is the curvature of the interface. Here, the factor 15 comes from the definition of the interface stiffness for a cubic crystal [16], where θ is the angle between the normal to the interface and the direction along which the growth is favored, i.e., the direction of minimum stiffness.

For the sake of readability, we refrain from giving further details on the boundary integral methods and refer to Refs. [21,22] and references therein for additional information. We mention that, apart from the shape of the interface, the steady-state velocity V is found, using the Ivantsov relation $\Delta = \sqrt{\pi P}\exp(P)\mathrm{erfc}\sqrt{P}$, where $P = \rho V/(2D_L)$ with ρ being the radius of the Ivantsov parabola [15]. The boundary integral technique has, up to now, only been used for the symmetric model ($\mu = 1$) and for the one-sided model ($\mu = 0$). This is probably due to the fact that for other values of μ, the number of unknowns that have to be found is doubled. Indeed, in addition to the shape of the interface, the normal gradient of the diffusion field at the interface should also be found self-consistently. However, the boundary integral equation was analyzed by Barbieri and Langer in Ref. [19], and it was shown that, in the limit of small anisotropy (in addition to being in the limit of small driving force Δ as usual in theoretical descriptions of weakly out-of-equilibrium dendritic growth), i.e., when the correcting term to the capillary length parametrized by 15ϵ in Eq. (9) is small, the steady-state velocity depends on μ in the following way:

$$\frac{V(\mu = 1)}{V(\mu)} = \frac{1 + \mu}{2}. \tag{10}$$

IV. RESULTS AND DISCUSSION

In this section, we present our results for an anisotropy strength $\epsilon = 0.04$. We benchmarked our nondiagonal PF model with GF calculations within the symmetric and one-sided models, for different values of the driving force Δ. The nondiagonal PF and chemical potential evolution equations presented in Eqs. (1) and (2) were iteratively solved in a two-dimensional simulation domain with a uniform grid spacing $\Delta x = \Delta y = 0.4 W_0$ by using an explicit finite-difference method. The sizes of the simulation domain were set to $L_x \times L_y = 768\Delta x \times 768\Delta y$ to $2048\Delta x \times 2048\Delta y$. To save the simulation time, only 1/4 dendrite was predefined at the left corner of the simulation domain with the far-field boundary condition $u \to \Delta$, and also a moving-frame method and GPU acceleration were employed in the present paper. Furthermore, we note that for the symmetric model where $D_S/D_L = 1$, the diffusivity is a constant, the cross-coupling parameter M vanishes and the classical PF model is recovered. For the one-sided case where $D_S/D_L = 0$, the diffusivity is given by Eq. (6), and the PF parameters are given by Eqs. (7) and (8).

In Table I, we gather our PF and GF results. We see that the PF model reproduces the GF results within 5% error, which is quite satisfactory, and no particular trend arises concerning the dependence of the error on Δ. On the other hand, we may state that the deviation shows a tendency to be larger for $\mu = 0$ than for $\mu = 1$.

TABLE I. Dimensionless steady-state velocity from the phase field simulations ($V_{\rm PF}$) and from the Green's function calculations ($V_{\rm GF}$). Here $\epsilon = 0.04$.

Δ	μ	$\frac{V_{\rm PF} d_0}{D_L}$	$\frac{V_{\rm GF} d_0}{D_L}$	Error (%)
0.65	1	0.0393	0.0399	1.5
	0	0.0573	0.0543	5.5
0.60	1	0.0238	0.0237	0.4
	0	0.0360	0.0344	4.7
0.55	1	0.0141	0.0139	1.4
	0	0.0219	0.0212	3.3
0.50	1	0.00817	0.00800	2.1
	0	0.0132	0.0126	4.8
0.45	1	0.00457	0.00443	3.2
	0	0.00744	0.00722	3.0

In the case $\epsilon = 0.04$, the correction to the capillary length in Eq. (9) is not much smaller than unity, and we see that the relation between the steady-state velocities for $\mu = 0$ and $\mu = 1$ does not follow Eq. (10). In Fig. 2, we present

$$\Omega = \frac{V(1)}{V(\mu)}\,\frac{2}{1 + \mu} \tag{11}$$

as a function of μ for our PF simulations (crosses), and for the analytical theory in Ref. [19] (horizontal black dashed line). The interface width for the PF simulations is chosen such that the velocity has converged with respect to the increasing ratio d_0/W_0, and the latter ranges from $d_0/W_0 = 0.139$ for the smallest velocities to $d_0/W_0 = 0.554$ for the largest ones.

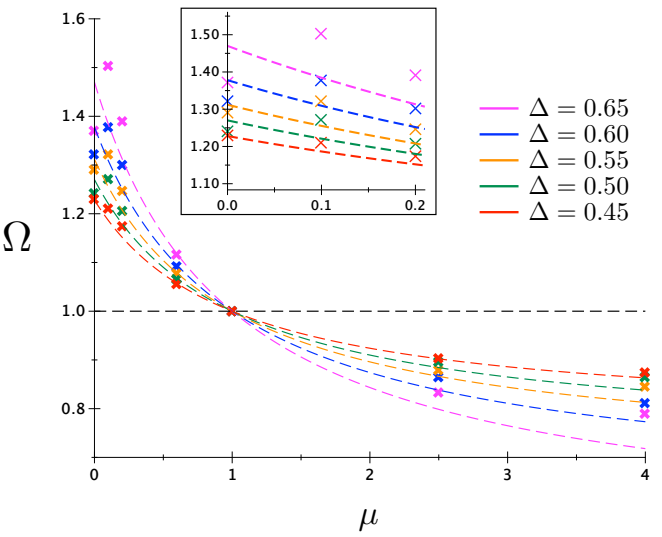

FIG. 2. Crosses: Rescaled ratio of velocities Ω [see Eq. (11) for definition] obtained from PF simulations as a function of μ, for different values of Δ; dashed colored lines: representation of Eq. (12) based on GF results for $\mu = 0$ and $\mu = 1$; black horizontal dashed line: Barbieri-Langer theory [19], i.e., Eq. (10).

We see that, although our PF simulations get closer to the analytical theory when Δ decreases, a large deviation remains, illustrating the breakdown of the assumptions made in Ref. [19]. Let us note that a relatively good agreement was found with the analytical theory for $\epsilon = 0.02$ and $\Delta = 0.55$ in Ref. [23]. However, the PF model developed in this paper, that was designed to account for diffusion in the growing phase, imposes an unjustified linear relationship between the fluxes at the interface and the interface velocity in addition to the conservation equation, and this model is therefore not consistent on the thermodynamic level.

Beyond reporting our PF results for the μ dependence of the dendrite-tip steady-state velocity, we propose now a generalization of the relation Eq. (10). This generalization aims at expressing the μ dependence of velocity for strengths of anisotropy for which the correction to the capillary length due to anisotropy in Eq. (9) is not small compared to unity, i.e., when $15\epsilon \simeq 1$. In view of the linear dependence of the ratio $V(\mu = 1)/V(\mu)$ in Eq. (10), we write

$$\frac{V(1)}{V(\mu)} = \frac{V(1)}{V(0)} + \mu\left[1 - \frac{V(1)}{V(0)}\right]. \tag{12}$$

This expression depends, apart from μ, on the ratio $V(1)/V(0)$. This ratio, that equals $1/2$ when Eq. (10) is recovered at small enough ϵ, is estimated for $\epsilon = 0.04$ using the velocities $V_{\mathrm{GF}}(\mu = 1)$ and $V_{\mathrm{GF}}(\mu = 0)$ obtained with the GF calculations for the symmetric and the one-sided model reported in Table I. In Fig. 2, Eq. (12) is then represented by the dashed colored lines, with each color corresponding to a different value of Δ. We clearly see that our PF calculations converge to Eq. (12) when Δ decreases. For $\Delta = 0.45$, the deviation between the PF results and Eq. (12) does not exceed 2%. When one additionally looks at the details of the curve in the neighborhood of $\mu = 0$ (in the inset), we observe that our PF results for $\Delta > 0.45$ exhibit an unexpected behavior. For $\mu = 0.1$ and 0.2, our PF results lie above Eq. (12), but they lie below for $\mu = 0$. We suspect that the form of the diffusivity function in Eq. (3), that involves the parameter a chosen such that surface diffusion is eliminated (let us note that other strategies have been used for such a purpose [24]), plays a role. Indeed, this function is nonmonotonous and the magnitude of its variations, that are restricted to region of width W, increases when the deviation of μ from unity increases. In comparison, for $\mu = 0$, the diffusivity in Eq. (6) provides the elimination of surface diffusion while being monotonous. Anyway, the PF results for the smallest value of Δ suggest that this unexpected behavior disappears when Δ is small enough.

The quality and robustness of the PF results presented above are supported by two other sets of simulations. For that, we have investigated the behavior of the PF model in the range $0 < \mu < 1$ when (1) the kinetic cross-coupling is turned off, i.e., when $M = 0$; and (2) the procedure to eliminate surface diffusion is turned off, i.e., when $a = 0$. We present in Fig. 3 the results for $\Delta = 0.55$ and $\Delta = 0.45$, together with the corresponding results already shown in Fig. 2. Let us note that the reference velocity $V(\mu = 1)$ is the same for case 1 ($M = 0$) and for case 2 ($a = 0$) because the diffusivity is a constant, i.e., $1/(2D_S) - 1/(2D_L) = 0$ in Eqs. (3) and (5). In both cases, we see that the results deviate from the PF results

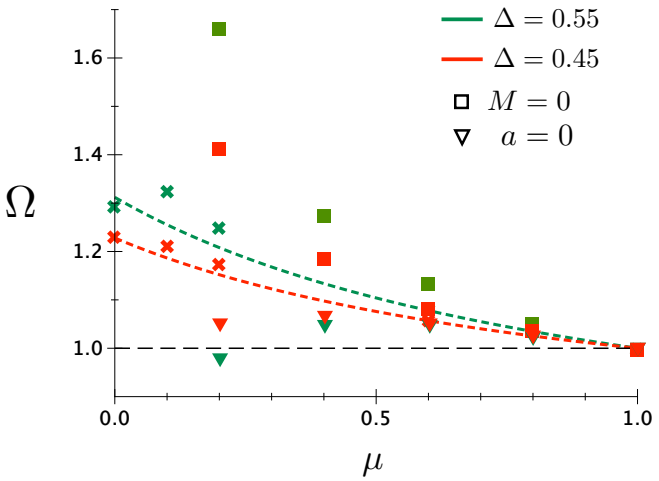

FIG. 3. Comparison between the nondiagonal PF results presented in Fig. 2 (crosses) and PF simulations with (1) squares: $M = 0$ and (2) triangles: $a = 0$. We evidence here the importance of the kinetic cross-coupling and the elimination of surface diffusion.

presented in Fig. 2. This deviation systematically increases when the deviation of μ from unity increases and when Δ increases. For example, for $\Delta = 0.45$, $\mu = 0.2$, this deviation approaches 20% when $M = 0$ and is larger than 10% when $a = 0$. These results therefore emphasize the necessity of using the nondiagonal PF model with elimination of surface diffusion. While the usage of a nondiagonal Onsager matrix of forces-flux relations is the elimination of surface diffusion is, here, necessary to achieve a quantitative agreement with the GF calculations in which surface diffusion is not included. In general, however, surface diffusion, in the sense of a tangential flux driven by variations of chemical potentials along the interface and leading to a normal motion of the latter (see Ref. [20] for more details), is allowed and takes place. Nevertheless, in the limit of small undercooling where the interface radius of curvature is large compared to the capillary length, the effect of surface diffusion is expected to be weak owing to the high order of the spatial derivatives that are involved in its description. The elimination of surface diffusion in the PF model, through the choice of a vanishing surface diffusion coefficient, is thus mainly designed so as to suppress effects that are enhanced due to the diffuseness of the interface.

We have also analyzed the dendrite tip region for $\Delta = 0.45$, $\epsilon = 0.04$. In Fig. 4(a), we present the steady-state dendritic shape obtained from PF simulations and from GF calculations for the symmetric and the one-sided cases. As expected from the small deviations reported in Table I, the dendrite shapes calculated by PF simulations in symmetric and one-sided cases agree perfectly with GF results. In Fig. 4(b), we present the dendritic shape close to the tip together with the Ivantsov parabola, for the simulation data presented in Fig. 2. For each μ, we rescale the dendrite shape by ρ, the radius of the Ivantsov parabola. The latter is obtained by plugging the growth velocity V obtained from simulation into the inverse Ivantsov relation, giving $P = \rho V/(2D_L)$ as a function of Δ. When we focus on a small region at a distance of approximately 1.5ρ behind the tip, we see that the scatter

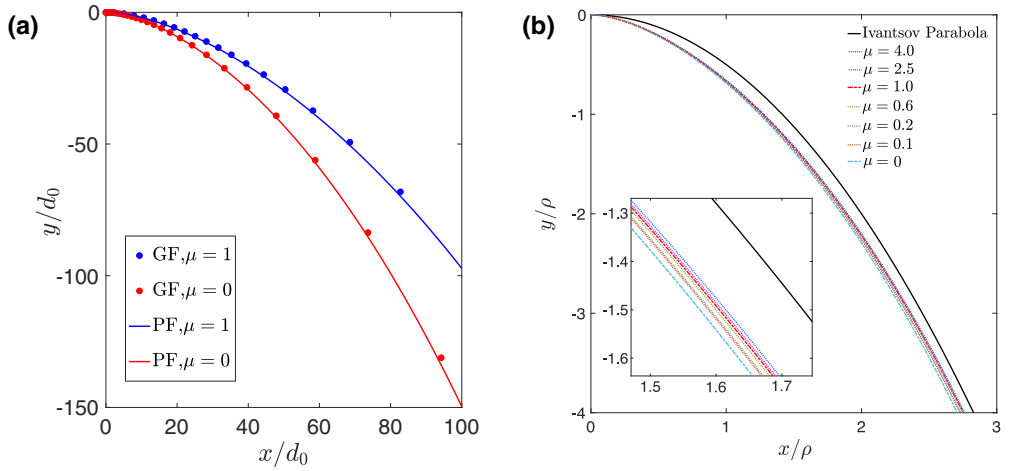

FIG. 4. (a) Comparison of the steady-state dendritic shapes obtained from PF simulations and the GF results for $\Delta = 0.45$ and $\epsilon = 0.04$ in symmetric and one-sided cases. (b) Interface position in the dendrite tip ($x = 0$) region scaled by the Ivantsov radius ρ for different values of μ and at $\Delta = 0.45$ and $\epsilon = 0.04$. The tip radius is weakly depending on μ when expressed in units of ρ.

of the position of the interface is rather small compared to the distance to the Ivantsov parabola. In comparison, in a simulation with $\epsilon = 0.01$, the position of the interface was much closer to the Ivantsov parabola, which is in line with the classical dendritic theory for which the tip converges to the Ivantsov parabola when the anisotropy of interface energy decreases. We may thus conclude from our study that the tip radius depends only weakly on μ when expressed in units of ρ.

Let us finally give a short remark on the case of large deviations from equilibrium. The one-sided PF model was recently investigated in the perspective of fast solidification [25], for which the boundary conditions for the chemical potentials jumps across the interface deviate from linear kinetics. Such an investigation would be valuable for the present model with diffusion in both phases. However, one should have in mind that our problem here is more complex that in the one-sided case. Indeed, in the latter, the absence of diffusion flux in the growing solid phase provides a constraint that is not present here (see the introduction in Ref. [10] for a more detailed discussion).

V. CONCLUSIONS

We have studied the capabilities of the nondiagonal PF model for the simulation of two-dimensional dendritic growth in the case where the diffusivity in the growing phase D_S neither vanishes nor equals the one of the disappearing phase D_L. While we have benchmarked our PF results with GF calculations (sharp-interface model) for $\mu = D_S/D_L = 0$ and $\mu = 1$, our calculations for other values of μ show significant deviations from the theory by Barbieri and Langer [19], in accordance with the expected breakdown of their assumptions for the strength of interface energy anisotropy that we have used in our simulations. In view of our results, we then propose a generalization of the prediction. We also have shown that an agreement between the PF model and GF method requires the kinetic cross-coupling and the elimination of surface diffusion. Our work opens up the way for quantitative PF simulations of phase transformations where diffusion in the growing phases plays an important role in the pattern and velocity selections.

Especially, assuming $D_S \neq 0$ and $D_S \neq D_L$ is adapted to the solidification and melting in pure materials, but also in interstitial alloys. The most obvious illustration for the latter case is given by the dendritic solidification of the δ ferrite in steels (see, for example, the recent Ref. [26]), for which the diffusion coefficient of interstitial carbon is comparable to the diffusion coefficient of carbon in the liquid phase. At lower temperatures, the diffusion of carbon in the δ ferrite drives the peritectic transformation, for which the austenite grows at the expense of the δ ferrite. For such a transformation, a PF model with a finite contrast of diffusion coefficient such as the one studied in this paper should be used. More generally, at temperatures well below the melting temperature, alloys usually present regions in their phase diagram where several solid phases coexist, and solid-state transformations such as eutectoid ones involve diffusion in all phases. In particular, it was shown that diffusion in the growing phases may have a significant influence on the eutectoid transformation velocity in the case where all diffusion coefficients are equal [14]. Our model thus provides the possibility to study such dependence in the general case with generically different nonvanishing diffusion coefficients.

ACKNOWLEDGMENTS

This work was supported by the China Scholarship Council (CSC) Grant No. 201706370221 and we thank the Deutsche Forschungsgemeinschaft (DFG) for funding via the Priority Program No. SPP 1713. One of the authors (G.B.) was supported by the German Federal Ministry of Education and Research (BMBF) in the framework of the Forschungscampus Digital Photonic Production: DPP Direct, FKZ Grant No. 13N13709.

[1] N. Provatas and K. Elder, *Phase-Field Methods in Materials Science and Engineering* (Wiley-VCH, Weinheim, Germany, 2010).

[2] G. Boussinot, Y. Le Bouar, and A. Finel, Phase-field simulations with inhomogeneous elasticity: Comparison with an atomic-scale method and application to superalloys, Acta Mater. **58**, 4170 (2010).

[3] D. M. Anderson, G. B. McFadden, and A. A. Wheeler, Diffuse-interface methods in fluid mechanics, Annu. Rev. Fluid Mech. **30**, 139 (1998).

[4] A. Karma and M. Plapp, Spiral Surface Growth without Desorption, Phys. Rev. Lett. **81**, 4444 (1998).

[5] R. Spatschek, M. Hartmann, E. Brener, H. Müller-Krumbhaar, and K. Kassner, Phase Field Modeling of Fast Crack Propagation, Phys. Rev. Lett. **96**, 015502 (2006).

[6] A. Karma and W. J. Rappel, Phase-field method for computationally efficient modeling of solidification with arbitrary interface kinetics, Phys. Rev. E **53**, R3017(R) (1996); Quantitative phase-field modeling of dendritic growth in two and three dimension, **57**, 4323 (1998).

[7] P. C. Hohenberg and B. I. Halperin, Theory of dynamic critical phenomena, Rev. Mod. Phys. **49**, 435 (1977).

[8] A. Karma, Phase-Field Formulation for Quantitative Modeling of Alloy Solidification, Phys. Rev. Lett. **87**, 115701 (2001).

[9] R. F. Almgren, Second-order phase field asymptotics for unequal conductivities, SIAM J. Appl. Math. **59**, 2086 (1999).

[10] G. Boussinot and E. A. Brener, Achieving realistic interface kinetics in phase-field models with a diffusional contrast, Phys. Rev. E **89**, 060402(R) (2014).

[11] E. A. Brener and G. Boussinot, Kinetic cross coupling between nonconserved and conserved fields in phase field models, Phys. Rev. E **86**, 060601(R) (2012).

[12] G. Boussinot and E. A. Brener, Interface kinetics in phase-field models: Isothermal transformations in binary alloys and step dynamics in molecular-beam epitaxy, Phys. Rev. E **88**, 022406 (2013).

[13] K. Nakajima, M. Apel, and I. Steinbach, The role of carbon diffusion in ferrite on the kinetics of cooperative growth of pearlite: A multi-phase field study, Acta Mater. **54**, 3665 (2006).

[14] K. Ankit, A. Choudhury, C. Qin, S. Schulz, M. McDaniel, and B. Nestler, Theoretical and numerical study of lamellar eutectoid growth influenced by volume diffusion, Acta Mater. **61**, 4245 (2013).

[15] G. P. Ivantsov, Temperature field around a spherical, cylindrical, and needle-shaped crystal, growing in a pre-cooled melt, Dokl. Akad. Nauk USSR **58**, 567 (1947).

[16] E. A. Brener and V. I. Mel'nikov, Pattern selection in two-dimensional dendritic growth, Adv. Phys. **40**, 53 (1991).

[17] E. Brener, Needle-crystal solution in three-Ddimensional dendritic growth, Phys. Rev. Lett. **71**, 3653 (1993).

[18] M. Ben Amar, E. Brener, M. Ben Amar, and E. Brener, Theory of Pattern Selection in Three-Dimensional Nonaxisymmetric Dendritic Growth, Phys. Rev. Lett. **71**, 589 (1993).

[19] A. Barbieri and J. S. Langer, Prediction of dendritic growth rates in the linearized solvability theory, Phys. Rev. A **39**, 5314 (1989).

[20] G. Boussinot, E. A. Brener, C. Hüter, and R. Spatschek, Elimination of surface diffusion in the non-diagonal phase field model, Continuum Mech. Thermodyn. **29**, 969 (2017).

[21] E. A. Brener, C. Hüter, D. Pilipenko, and D. E. Temkin, Velocity Selection Problem in the Presence of the Triple Junction, Phys. Rev. Lett. **99**, 105701 (2007).

[22] Y. Saito, G. Goldbeck-Wood, and H. Müller-Krumbhaar, Numerical simulation of dendritic growth, Phys. Rev. A **38**, 2148 (1988).

[23] M. Ohno and K. Matsuura, Quantitative phase-field modeling for dilute alloy solidification involving diffusion in the solid, Phys. Rev. E **79**, 031603 (2009).

[24] M. Ohno, T. Takaki, and Y. Shibuta, Variational formulation and numerical accuracy of a quantitative phase-field model for binary alloy solidification with two-sided diffusion, Phys. Rev. E **93**, 012802 (2016).

[25] T. Pinomaa and N. Provatas, Quantitative phase field modeling of solute trapping and continuous growth kinetics in quasi-rapid solidification, Acta Mater. **168**, 167 (2019).

[26] H. Yasuda, K. Morishita, N. Nakatsuka, T. Nishimura, M. Yoshiya, A. Sugiyama, K. Uesugi, and A. Takeuchi, Dendrite fragmentation induced by massive-like δ–γ transformation in Fe–C alloys, Nat. Commun. **10**, 3183 (2019).